organics

Article

Bis(3-methylthio-1-azulenyl)phenylmethyl Cations and Dications Connected by a 1,4-Phenylene Spacer: Synthesis and Their Electrochemical Properties

Taku Shoji [1,2,*], Naoko Sakata [2], Ryuta Sekiguchi [3] and Shunji Ito [3]

1 Department of Chemical Biology and Applied Chemistry, College of Engineering, Nihon University, Koriyama 963-8642, Japan
2 Department of Material Science, Graduate School of Science and Technology, Shinshu University, Matsumoto 390-8621, Japan
3 Graduate School of Science and Technology, Hirosaki University, Hirosaki 036-8561, Japan
* Correspondence: shoji.taku@nihon-u.ac.jp; Tel.: +81-24-956-8808

Abstract: The preparation of bis(3-methylthio-1-azulenyl)phenylmethyl cations and 1,4-phenylene bis[bis(3,6-di-*tert*-butyl-1-azulenyl)methyl] dications was accomplished by the hydride abstraction of the corresponding hydride derivatives, which were synthesized by the acid-catalyzed condensation of 1-azulenyl methyl sulfide with benzaldehyde and terephthalaldehyde with 2,3-dichloro-5,6-dicyano-1,4-benzoquinone. The intramolecular charge transfer among the azulene ring and the methylium moieties of these cations and dications was investigated by UV–Vis spectroscopy and electrochemical analyses. The p$K_R{}^+$ values of the cations were examined for their thermodynamic stability spectrophotometrically. The voltammetry experiments of these cations revealed their reversible reduction waves on their cyclic voltammograms. Moreover, a notable spectral change of cations was observed by spectroelectrochemistry during electrochemical reduction conditions.

Keywords: azulene; carbocation; redox system

Citation: Shoji, T.; Sakata, N.; Sekiguchi, R.; Ito, S. Bis(3-methylthio-1-azulenyl)phenylmethyl Cations and Dications Connected by a 1,4-Phenylene Spacer: Synthesis and Their Electrochemical Properties. *Organics* **2022**, *3*, 507–519. https://doi.org/10.3390/org3040034

Academic Editors: Wim Dehaen, Michal Szostak and Huaping Xu

Received: 24 October 2022
Accepted: 9 December 2022
Published: 16 December 2022

1. Introduction

Azulene and its derivatives have attracted interest in terms of their specific optical properties [1–6] and pharmacological activity [7–10]. The azulene system significantly stabilizes cationic as well as anionic states through the contribution of tropylium and cyclopentadienide substructures. Utilizing this characteristic property, the synthesis of redox-active chromophores composed by the azulene derivatives has been employed in our group due to the creation of stabilized electrochromic materials [11–21]. As a part of this research, a high thermodynamic stability and reversible redox behavior under the electrochemical conditions were observed in bis(1-azulenyl)phenylmethyl cations and dications connected by a 1,4-phenylene spacer, namely, $\mathbf{1}^+$ and $\mathbf{2}^{2+}$ (Figure 1) [11,12,22]. However, in spectroelectrochemical measurements, $\mathbf{1}^+$ and $\mathbf{2}^{2+}$ showed significant decomposition under electrochemical reduction conditions.

Previously, we have described the effective synthetic procedure of several 1-azulenyl sulfides, as well as their unique reactivity and properties [23–28]. In these studies, we found that 1-azulenyl sulfides exhibit remarkable redox stability toward the electrochemical reactions. Considering these results, cations and dications incorporating the 1-methylthioazulene moieties should improve electrochemical stability in the electrochromic systems, i.e., having high reversibility in the redox behavior, in addition to a large thermodynamic stability in the ionic states.

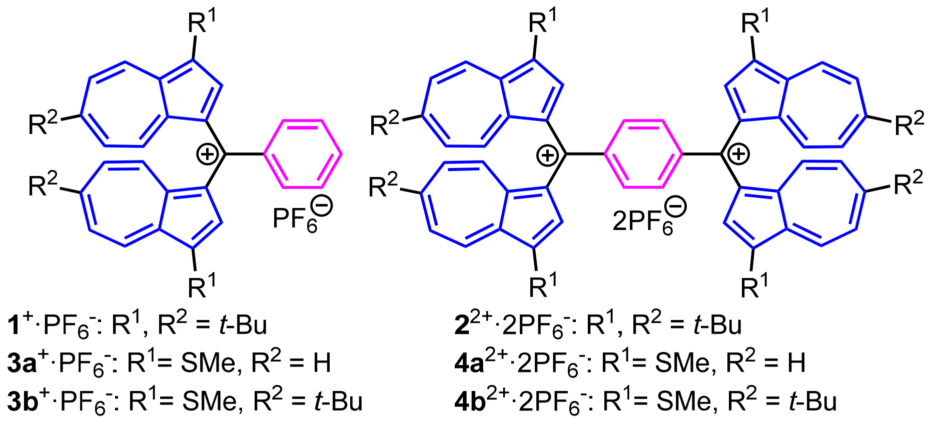

Figure 1. Structures of bis(1-azulenyl)phenylmethylium hexafluorophosphates: $\mathbf{1}^{+}\cdot PF_6^-$ and $\mathbf{3a,b}^{+}\cdot PF_6^-$ and 1,4-phenylenebis[bis(1-azulenyl)methylium] bis(hexafluorophosphate)s; $\mathbf{2}^{2+}\cdot 2PF_6^-$ and $\mathbf{4a,b}^{2+}\cdot 2PF_6^-$.

We describe herein the preparation of bis(3-methylthio-1-azulenyl)phenylmethyl cations $\mathbf{3a,b}^{+}\cdot PF_6^-$ and dications $\mathbf{4a,b}^{2+}\cdot 2PF_6^-$ connected by a 1,4-phenylene spacer. The thermodynamic stability of cations $\mathbf{3a,b}^{+}\cdot PF_6^-$ and dications $\mathbf{4a,b}^{2+}\cdot 2PF_6^-$ were measured spectrophotometrically. Their redox behavior, as examined by cyclic voltammetry (CV) and differential pulse voltammetry (DPV), were also discussed. The spectroelectrochemistry of these cations was also examined, which showed notable spectral changes in the visible region in different redox states.

2. Results and Discussion

Synthesis: The strategy of reacting the aldehydes with azulene derivatives under acidic conditions to obtain the condensation product has been reported previously by several researchers, including our group [29–35]. The synthesis of bis(3-methylthio-1-azulenyl)methylbenzenes **6a**,**b** was accomplished by the condensation of **5a**,**b** **[23]** with benzaldehyde in acetic acid (AcOH), followed by the usual workup process in 93% and 100% yields, respectively (Figure 2). The higher reaction yields are considered to be due to the reaction control by the methyl sulfide group at the 1-position of the azulene ring, which suppresses the undesired oligomerization reactions occurring at both the 1- and 3-positions [36,37]. Compounds **7a**,**b** were obtained in 87% and 95% yields by the reaction of **5a**,**b** with terephthalaldehyde in a similar manner (Figure 2).

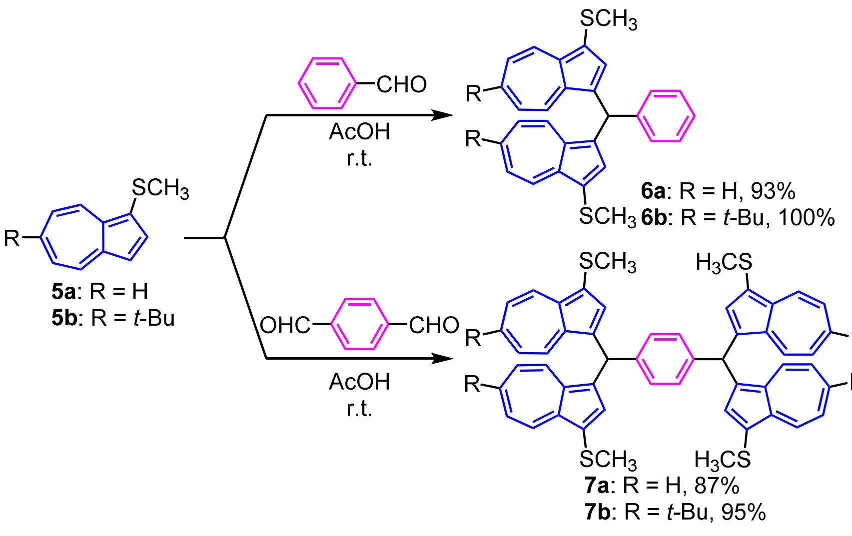

Figure 2. Synthesis of **6a**,**b** and **7a**,**b** from 1-methylthioazulenes **5a**,**b**.

The synthesis of **3a**,**b**$^{+}$·PF_6^{-} and **4a**,**b**$^{2+}$·$2PF_6^{-}$ was established by the reaction of **6a**,**b**, and **7a**,**b** with 2,3-dichloro-5,6-dicyano-1,4-benzoquinone (DDQ), as shown in Figure 3. The reactions of **6a** and **6b** with DDQ in dichloromethane (CH_2Cl_2), followed by the treatment with 60% HPF_6 solution, produced **3a**$^{+}$·PF_6^{-} and **3b**$^{+}$·PF_6^{-} in 99% and 91% yield, respectively (Figure 3). Similar to the synthesis of **3a**,**b**$^{+}$·PF_6^{-}, the hydride abstraction of **7a**,**b** with a two-fold amount of DDQ gave the dications **4a**,**b**$^{2+}$·$2PF_6^{-}$ in 91% and 99% yields, after the addition of aq. HPF_6 (Figure 3).

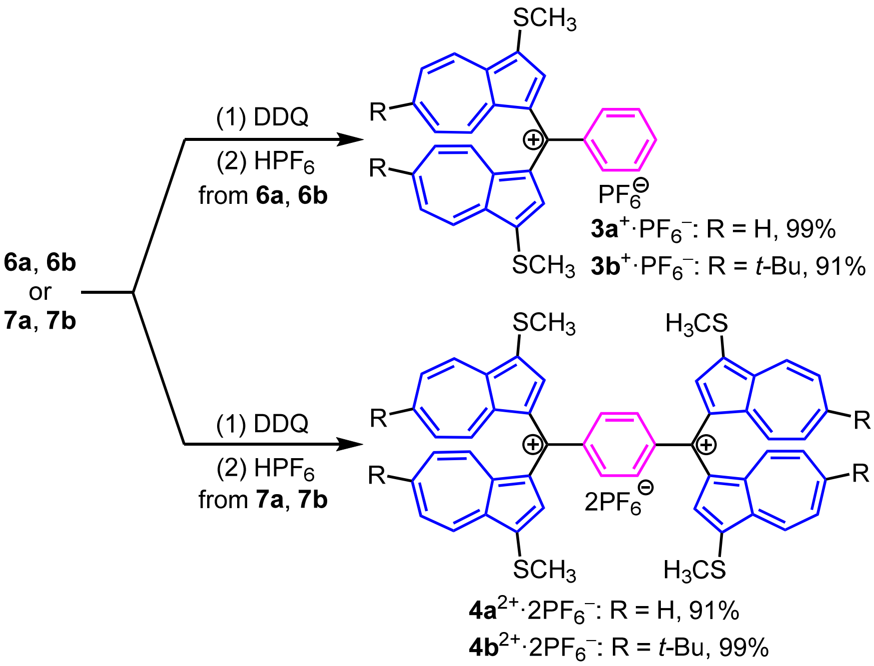

Figure 3. Synthesis of cation **3a**,**b**$^{+}$·PF_6^{-} and dications **4a**,**b**$^{2+}$·$2PF_6^{-}$.

Spectroscopic properties: Cations **3a**,**b**$^{+}$·PF_6^{-} and **4a**,**b**$^{2+}$·$2PF_6^{-}$ were fully characterized by spectroscopic data, as appears in the "Materials and Methods" section. High-resolution mass spectra (HRMS) revealed the correct molecular ion peaks. The chemical shifts in ^{1}H NMR spectra of the azulene moiety for **3a**,**b**$^{+}$·PF_6^{-} and **4a**,**b**$^{2+}$·$2PF_6^{-}$ revealed low-field shifts compared with those of **6a**,**b** and **7a**,**b,** attributing to the electron-withdrawing property of the methylium ion attached.

As expected by their cationic structures, UV–Vis spectra of **3a**,**b**$^{+}$·PF_6^{-} and **4a**,**b**$^{2+}$·$2PF_6^{-}$ displayed the characteristic strong absorption band in the visible region (Table 1). For instance, the UV–Vis spectra of **3a**,**b**$^{+}$·PF_6^{-} and **4a**,**b**$^{2+}$·$2PF_6^{-}$ in MeCN showed an absorption band at λ_{max} = 740 nm (**3a**$^{+}$·PF_6^{-}), 738 nm (**3b**$^{+}$·PF_6^{-}), 773 nm (**4a**$^{2+}$·$2PF_6^{-}$), and 766 nm (**4b**$^{2+}$·$2PF_6^{-}$), which spread into the near-infrared region. The absorption maxima of **4a**,**b**$^{2+}$·$2PF_6^{-}$ showed a modest red shift compared with those of **3a**,**b**$^{+}$·PF_6^{-}, implying the expansion of the π-electron system through the 1,4-phenylene spacer. The molar absorption coefficients of **4a**,**b**$^{2+}$·$2PF_6^{-}$ are approximately twice as large as those of **3a**,**b**$^{+}$·PF_6^{-}, owing to the two bis(1-azulenyl)methylium units substituted. The strong and broad absorption bands of these cations can be ascribed to intramolecular charge transfer (ICT) across the two azulene rings, as illustrated by the resonance structure (Figure 4).

Table 1. The longest absorption maxima [nm] and their coefficients (log ε) of **3a,b**$^+$·PF_6^- and **4a,b**$^{2+}$·2PF_6^- in several solvents, and those of **1**$^+$·PF_6^- and **2**$^{2+}$·2PF_6^- in acetonitrile (MeCN) as a reference.

	λ_{max}, nm (log ε)		
Compound	**CH_2Cl_2**	**MeCN**	**Hexane** [a]
3a$^+$·PF_6^-	755 (4.44)	740 (4.44)	732 (4.42)
3b$^+$·PF_6^-	740 (4.40)	738 (4.44)	723 (4.38)
4a^{2+}·2PF_6^-	785 (4.55)	773 (4.55)	– [b]
4b^{2+}·2PF_6^-	777 (4.54)	766 (4.62)	766 (4.44)
1$^+$·PF_6^- [22]	–	681 (4.61)	–
2^{2+}·2PF_6^- [22]	–	703 (4.85)	–

[a] 10% CH_2Cl_2 was added to maintain the solubility. [b] The longest absorption maxima in this solvent could not be determined since the absorption band was broadened into the near-infrared region.

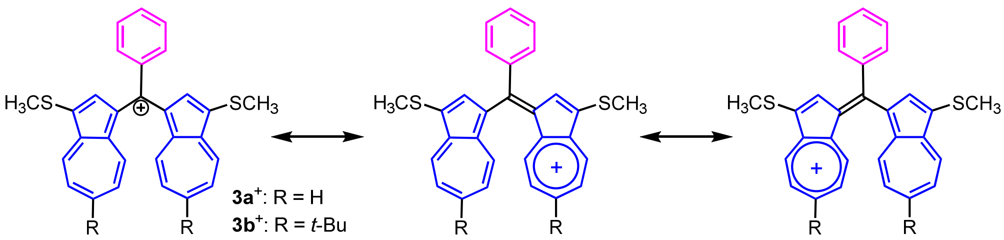

Figure 4. Plausible resonance structures of **3a,b**$^+$·PF_6^-.

Solvatochromism is one of the characteristic features of dipolar molecules [38–40]. The solvent dependence of the UV–Vis spectra in the visible region of **3a,b**$^+$·PF_6^- and **4a,b**$^{2+}$·2PF_6^- implied the ICT character of the absorption band. A strong absorption band of **3a**$^+$·PF_6^- at λ_{max} = 755 nm in CH_2Cl_2 showed a hypsochromic shift to λ_{max} = 732 nm in the less-polar solvent, i.e., in 10% CH_2Cl_2/hexane-mixed solvent (Figure 5). Similar solvent effects observed in CH_2Cl_2 and 10% CH_2Cl_2/hexane in **3a**$^+$·PF_6^- can also be observed in **3b**$^+$·PF_6^- and **4a,b**$^{2+}$·2PF_6^-.

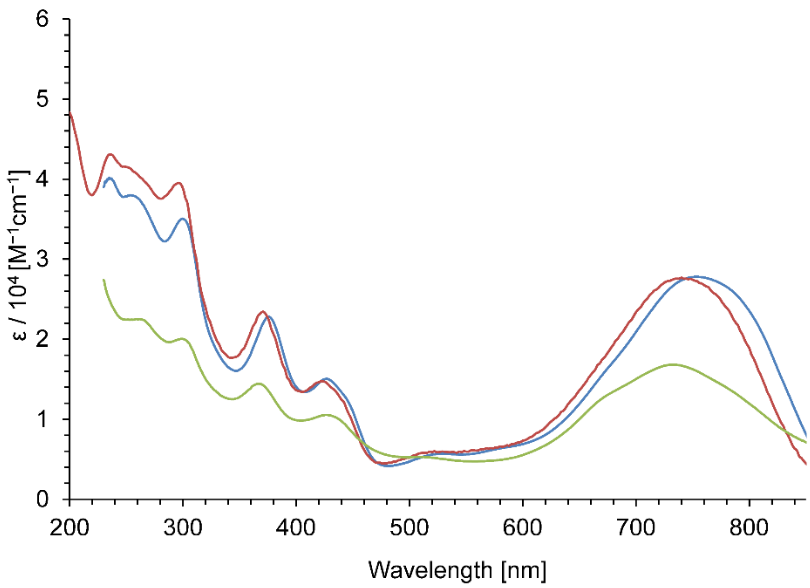

Figure 5. UV–Vis spectra of **3a**$^+$·PF_6^- in CH_2Cl_2 (blue line), in MeCN (red line), and in 10% CH_2Cl_2/hexane (light green line).

The p$K_R$$^+$ values of **3a,b**$^+$·PF_6^- and **4a,b**$^{2+}$·2PF_6^- were measured spectrophotometrically to investigate the thermodynamic stability of the cations (Table 2). The p$K_R$$^+$ value of **3b**$^+$·PF_6^- (pK_R^+ = 11.6 ± 0.1) was higher than that of **3a**$^+$·PF_6^- (pK_R^+ = 9.9 ± 0.1). These outcomes could be ascribed to the stabilization by the hyperconjugation of the *tert*-butyl group at the seven-membered moiety of the azulene ring [23]. The **4a**$^{2+}$·2PF_6^- (pK_R^+ = 9.8 ± 0.1) and **4b**$^{2+}$·2PF_6^- (pK_R^+ = 11.7 ± 0.1) with two cation units were neutralized simultaneously. Thus, **4a**$^{2+}$·2PF_6^- and **4b**$^{2+}$·2PF_6^- exhibit high stability, as similar to those of **3a**$^+$·PF_6^- and **3b**$^+$·PF_6^-. The pK_R^+ values of **3a**$^+$·PF_6^- and **3b**$^+$·PF_6^- are lower than that of **1**$^+$·PF_6^- (pK_R^+ = 12.4). These outcomes indicate that the stabilization by the methylthio group is less effective than the *tert*-butyl group, which is most likely attributed to the ineffective electron-donating ability of the sulfur atom.

Table 2. pK_R^+ Values [a] of **3a,b**$^+$·PF_6^-, **4a,b**$^{2+}$·2PF_6^-, **1**$^+$·PF_6^-, and **2**$^{2+}$·2PF_6^-.

Sample	pK_R^+	Sample	pK_R^+
3a$^+$·PF_6^-	9.9 ± 0.1	**4a**$^{2+}$·2PF_6^-	9.8 ± 0.1
3b$^+$·PF_6^-	11.6 ± 0.1	**4b**$^{2+}$·2PF_6^-	11.7 ± 0.1
1$^+$·PF_6^- [22]	12.4	**2**$^{2+}$·2PF_6^- [22]	12.1 ± 0.2

[a] The pK_R^+ values were determined spectrophotometrically in a buffer solution prepared in 50% aqueous MeCN.

The redox behaviors of **3a,b**$^+$·PF_6^- and **4a,b**$^{2+}$·2PF_6^- were investigated by CV and DPV, in order to clarify their electrochemical properties (Table 3). Cation **3a**$^+$·PF_6^- revealed a reversible reduction wave at E_1^{red} = −0.60 V on the CV, indicating the generation of a neutral radical species (Figure 6). The half-wave potential of E_1^{red} = –0.68 V on the CV was observed in the electrochemical reduction of **3b**$^+$·PF_6^-. The E_1^{red} value of **3b**$^+$·PF_6^- showed a slight cathodic shift compared with that of **3a**$^+$·PF_6^-, indicating the stabilization of the carbocation by the *tert*-butyl groups, as expected from the results of the pK_R^+ measurements.

Table 3. Redox Potentials [a] of **3a,b**$^+$·PF_6^-, **4a,b**$^{2+}$·2PF_6^-, **1**$^+$·PF_6^-, and **2**$^{2+}$·2PF_6^- in benzonitrile.

Sample	Method	E_1^{red} [V]	E_2^{red} [V]	E_1^{ox} [V]	E_2^{ox} [V]
3a$^+$·PF_6^-	CV	–0.60			
	(DPV)	(–0.59)	(–1.71)	(+0.65)	(+0.96)
3b$^+$·PF_6^-	CV	–0.68			
	(DPV)	(–0.66)	(–1.45)	(+0.64)	(+0.97)
4a^{2+}·2PF_6^-	CV	–0.35			
	(DPV)	(–0.33)	(–1.65)	(+0.67)	
4b^{2+}·2PF_6^-	CV	–0.42		+0.65	
	(DPV)	(–0.40)	(–1.74)	(+0.63)	
1$^+$·PF_6^- [23] [b]	CV [b]	–0.78		+0.88	
2^{2+}·2PF_6^- [23] [b]	CV [b]	–0.55		+0.87	

[a] Redox potentials were measured by CV and DPV [V vs. Ag/$AgNO_3$, 1 mM in benzonitrile containing Et_4NClO_4 (0.1 M), Pt electrode (i.d.: 1.6 mm), scan rate = 100 mV s^{-1}, and Fc/Fc^+ = +0.15 V]. In the case of reversible waves, half-wave potentials measured by CV are presented. The peak potentials measured by DPV are shown in parentheses. [b] Measured in MeCN containing Et_4NClO_4 (0.1 M) and Fc/Fc^+ = +0.07 V.

Although the pK_R^+ values are almost equal each other, the E_1^{red} of **4a**$^{2+}$·2PF_6^- (E_1^{red} = –0.35 V) displayed a more anodic shift than that of **3a**$^+$·PF_6^- (E_1^{red} = –0.60 V). The anodic shift of **4a**$^{2+}$·2PF_6^- may be ascribed to the electrochemical instability resulting from the electrostatic repulsion between the cations through the benzene ring connected. The reversible reduction waves of **4a,b**$^{2+}$·2PF_6^- may be attributable to the one-step reduction of the two cation units forming the closed-shell quinoidal structures **8a** and **8b**, as shown in Figure 7 [41].

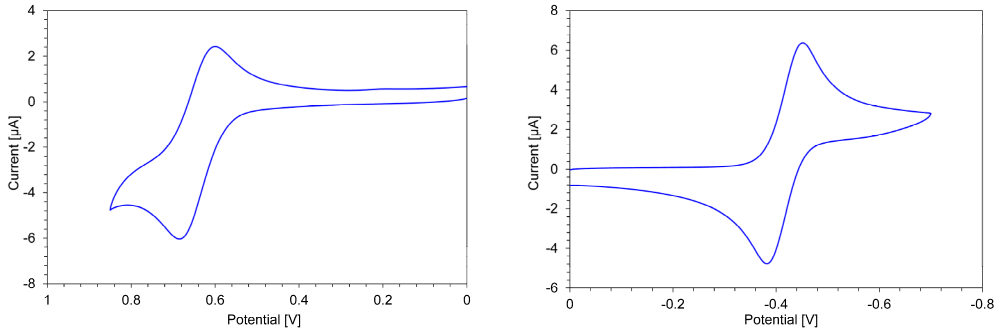

Figure 6. Cyclic voltammogram for the oxidation (**left**) and reduction (**right**) of $\mathbf{4b}^{+}\cdot PF_6^{-}$ in benzonitrile (1 mM) containing Et_4NClO_4 (0.1 M) as a supporting electrolyte.

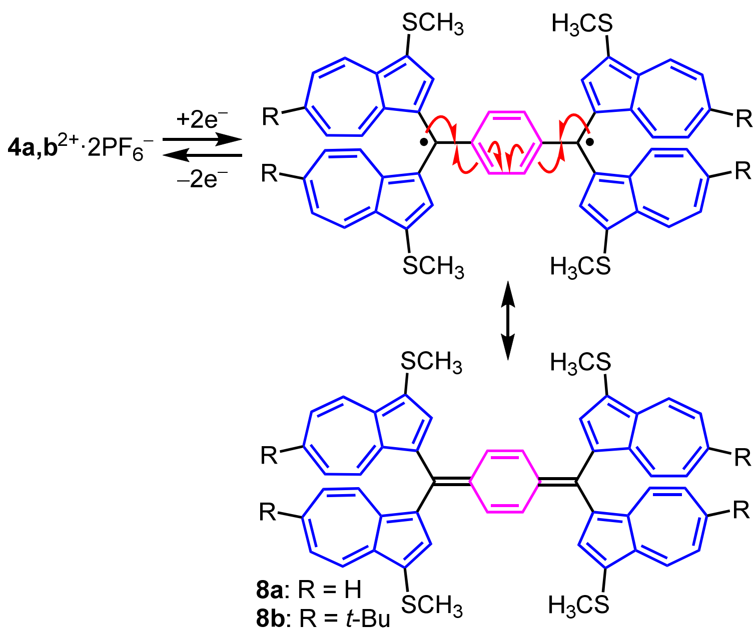

Figure 7. Plausible redox behavior of $\mathbf{4a,b}^{2+}\cdot 2PF_6^{-}$ and generated quinoidal species **8a**,**b**.

Electrochromism is a phenomenon that displays a significant color change in different redox states and is observed in molecules that show reversible redox behavior. Since high redox stability is required for the application to electrochromic materials, durability toward the redox cycle is an important factor to construct such materials [42–44]. The concept of violene–cyanine hybrids was proposed by Hünig et al. as a guideline for the creation of electrochromic materials [45–49]. The hybrid consists of a violene substructure involving delocalized, closed-shell polymethine (e.g., cyanine) dyes as terminal groups. Thus, in a redox system with a hybrid structure, the color of the cyanine dye could be observed by overall two-electron transfer (Figure 8). In contrast to the violene-type redox system, hybrid structures should improve the stability of electrochromic systems because both colored and discolored species comprise a closed shell structure.

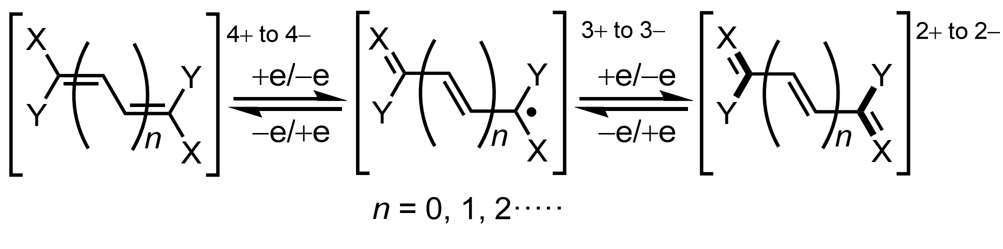

Figure 8. The general structure of violene–cyanine hybrids proposed by Hünig et al.; cyanine-type substructures produced by two-electron transfer are illustrated by bold lines.

Therefore, spectroelectrochemical measurements of **3a**,**b**$^{+}$·PF_6^{-} and **4a**,**b**$^{2+}$·$2PF_6^{-}$ were investigated under an electrochemical reaction. In the electrochemical reduction, the longest absorption band of λ_{max} = 740 nm for **3a**$^{+}$·PF_6^{-} gradually decreased, at which time the color of the solution changed from green to yellow. However, despite the good reversibility observed on the CV, the reverse oxidation of the yellow-colored solution did not reproduce the original spectrum of **3a**$^{+}$·PF_6^{-} (27% recovery, Figure 9). The less reversible color change might be explained by the generation of unstable neutral radical species under the measurement conditions. The absorption band at λ_{max} = 738 nm of **3b**$^{+}$·PF_6^{-} was also reduced upon the electrochemical reduction, along with the green-colored solution turning to yellow (see Supplementary Materials). Similar to **3a**$^{+}$·PF_6^{-}-, the visible spectrum of **3b**$^{+}$·PF_6^{-} was incompletely recovered when the reduced solution was reversely oxidized (12% recovery).

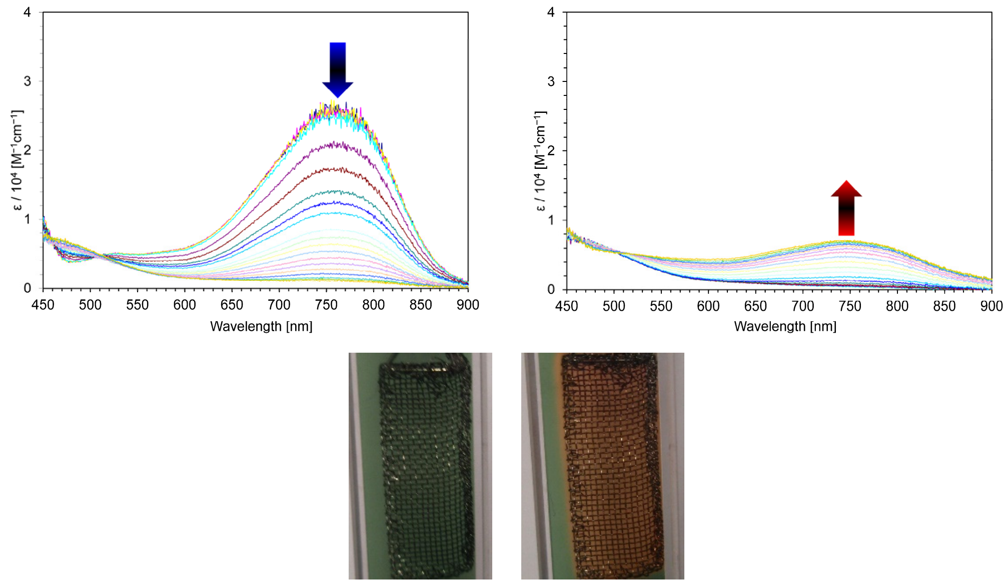

Figure 9. Continuous change in visible spectra of **3a**$^{+}$·PF_6^{-} in benzonitrile containing Et_4NClO_4 (0.1 M): constant-current electrochemical reduction (50 µA) at 30 s intervals (**left**) and the reverse oxidation (**right**) of the reduced species (50 µA) at 30 s intervals. Photo: Color changes of **3a**$^{+}$·PF_6^{-} upon the electrochromic analysis in benzonitrile containing Et_4NClO_4 (0.1 M) (50 µA); before electrochemical reduction (**left**) and after electrochemical reduction (**right**).

The color change of **4a**,**b**$^{2+}$·$2PF_6^{-}$ was also observed under the electrochemical reduction. In the absorption spectrum of **4a**,**b**$^{2+}$·$2PF_6^{-}$, an absorption band was developed at around λ_{max} = 600 nm during the electrolytic reduction, accompanied by the disappearance of the absorption band centered at λ_{max} = 773 nm. The original absorption spectrum of **4a**$^{2+}$·$2PF_6^{-}$ was regenerated by the reverse oxidation of the reducing species (51% recovery) (see Supplementary Materials). This reversible spectral change was also confirmed by the electrochemical reduction of **4b**$^{2+}$·$2PF_6^{-}$, with a gradual development of the absorption band at around λ_{max} = 610 nm, resulting in the green color of the solution turning blue. Reverse oxidation resulted in the disappearance of the newly generated absorption band, together with the regeneration of the original absorption of **4b**$^{2+}$·$2PF_6^{-}$ (64% recovery, Figure 10). The higher reversibility of **4a**,**b**$^{2+}$·$2PF_6^{-}$, compared to that of **3a**,**b**$^{+}$·PF_6^{-}, could be explained by the generation of closed-shell species, i.e., quinoidal species **8a**,**b**, by electrochemical reduction.

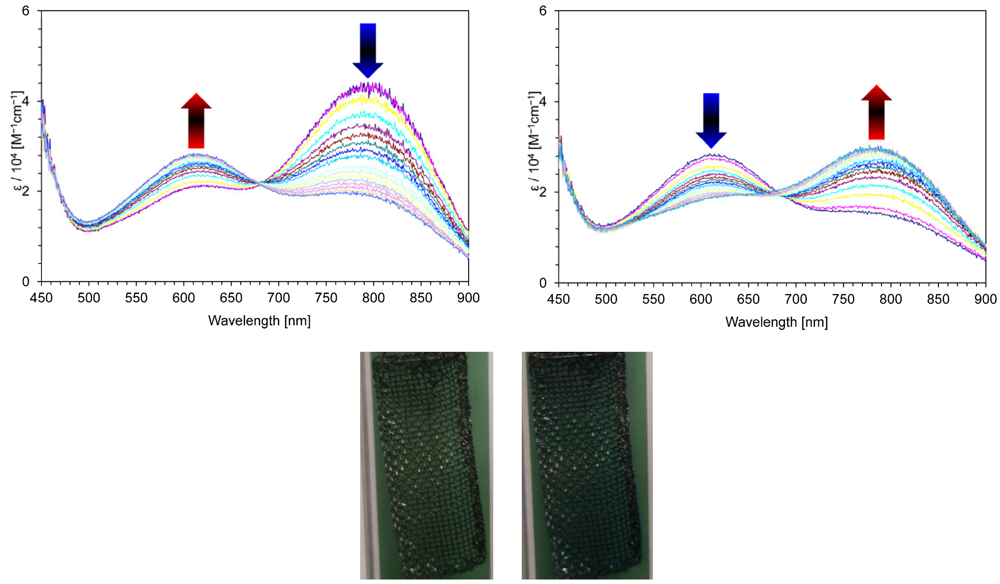

Figure 10. Continuous change in visible spectra of $\mathbf{4b^{2+}}{\cdot}2PF_6^-$ in benzonitrile containing Et_4NClO_4 (0.1 M): constant-current electrochemical reduction (50 μA) at 30 s intervals (**top**) and the reverse oxidation (**bottom**) of the reduced species (50 μA) at 30 s intervals. Photo: Color changes of $\mathbf{4a^{2+}}{\cdot}2PF_6^-$ upon the electrochromic analysis in benzonitrile containing Et_4NClO_4 (0.1 M) (50 μA); before electrochemical reduction (**left**) and after electrochemical reduction (**right**).

Dications $\mathbf{4a,b^{2+}}{\cdot}2PF_6^-$ contain two bis(3-methylthio-1-azulenyl)methylium units as the end groups, which are regarded as cyanine-type substructures to form a delocalized closed-shell system in the violene–cyanine hybrid structure. Thus, the electrochemical reduction of $\mathbf{4a,b^{2+}}{\cdot}2PF_6^-$ could generate the other closed-shell systems **8a**,**b** by two-electron transfer. As seen from the electrochemical behavior of $\mathbf{4a,b^{2+}}{\cdot}2PF_6^-$, the radical cationic species are not important in the redox systems, so the color change in the absorption spectra is mainly due to these two closed-shell species throughout. Since the dications $\mathbf{4a,b^{2+}}{\cdot}2PF_6^-$ displayed distinct spectral changes at the different redox states, the electrochromic behavior of these dications should serve as the violene–cyanine hybrid, in which the four end groups X and Y in Figure 8 are azulene rings to form a quinoidal substructure in their reduced form.

3. Materials and Methods

Melting points were measured with a Yanagimoto MPS3 micro melting apparatus. High-resolution mass spectra were obtained with a Bruker APEX II instrument. IR spectra were measured with a JASCO FT/IR-4100 spectrophotometer (JASCO Corporation, Tokyo, Japan). The UV–Vis spectra were recorded with a Shimadzu UV-2550 spectrophotometer (Shimadzu Corporation, Kyoto, Japan). ^1H and ^{13}C NMR spectra were recorded in $CDCl_3$ with a Bruker Avance 400 at 400 MHz and 100 MHz (Bruker BioSpin, Rheinstetten, Germany), respectively.

Bis(3-methylthio-1-azulenyl)phenylmethane (**6a**): a mixture of **5a** (273 mg, 1.57 mmol) and benzaldehyde (55 mg, 0.52 mmol) in acetic acid (5 mL) was stirred at room temperature for 24 h. The reaction mixture was diluted with CH_2Cl_2. The organic layer was washed with a 5% $NaHCO_3$ solution and water, dried over $MgSO_4$, and concentrated under reduced pressure. The residue was purified by column chromatography on silica gel with CH_2Cl_2 to afford **6a** (212 mg, 93%) as greenish-blue crystals. M.p. 186.0–188.0 °C (CH_2Cl_2); IR (KBr disk): ν_{max} = 3021 (w), 2915 (w), 1574 (s), 1493 (m), 1451 (w), 1399 (s), 1381 (m), 1333 (w), 1248 (w), 1129 (w), 1075 (w), 1030 (w), 945 (w), 914 (w), 878 (w), 862 (w), 737 (s), 706 (m), 573 (w), 561 (w) cm^{-1}; UV–Vis (CH_2Cl_2): λ_{max} (log ε) = 240 (4.60), 296 sh (4.75), 299 (4.76), 366 sh (4.02), 374 (4.06), 619 (2.67) nm; ^1H NMR (400 MHz, $CDCl_3$): δ = 8.44 (d, 2H, *J* = 9.6 Hz, H-4), 8.04 (d, 2H, *J* = 9.6 Hz, H-8), 7.36 (s, 2H, H-2), 7.32 (t, 2H, *J* = 9.6 Hz, H-6), 7.14–7.02 (m, 5H, Ph), 6.98 (t, 2H, *J* = 9.6 Hz, H-5), 6.80 (d, 2H, *J* = 9.6 Hz, H-7), 6.54 (s, 1H, CH), 2.22 ppm (s, 6H, SCH_3); ^{13}C NMR (100 MHz, $CDCl_3$): δ = 145.37, 141.33, 140.10, 138.90, 137.16, 135.93, 134.48, 132.67, 129.27, 128.92, 126.74, 123.45, 123.42, 120.85, 43.14, 20.99 ppm; HRMS (ESI): Calculated for $C_{29}H_{24}S_2 + Na^+$ $[M + Na]^+$ 459.1212; found: 459.1211.

Bis(6-*tert*-butyl-3-methylthio-1-azulenyl)phenylmethane (**6b**): the procedure used for the preparation of **6a** was adopted here. Reaction of 5**b** (1.00 g, 4.34 mmol) and benzaldehyde (185 mg, 1.74 mmol) in acetic acid (15 mL) at room temperature for 24 h, followed by column chromatography on silica gel with CH_2Cl_2 to afford **6b** (660 mg, 100%) as a blue solid. M.p. 152.0–155.0 °C (CH_2Cl_2); IR (KBr disk): ν_{max} = 2965 (m), 2869 (w), 1580 (s), 1493 (w), 1408 (w), 1397 (m), 1364 (w), 1306 (w), 1254 (w), 1067 (w), 963 (w), 839 (w), 716 (w), 698 (w), 677 (w), 581 (w) cm^{-1}; UV–Vis (CH_2Cl_2): λ_{max} (log ε) = 241 (4.60), 305 (4.91), 360 (4.07), 376 (4.08), 600 (2.87) nm; ^{1}H NMR (400 MHz, $CDCl_3$): δ = 8.51 (d, 2H, *J* = 10.4 Hz, H-8), 8.12 (d, 2H, *J* = 10.4 Hz, H-4), 7.38 (s, 2H, H-2), 7.34 (dd, 2H, *J* = 10.4, 1.6 Hz, H-7), 7.17 (dd, 2H, *J* = 10.4, 1.6 Hz, H-5), 7.3–7.1 (m, 5H, Ph), 6.60 (s, 1H, CH), 2.35 (s, 6H, SCH_3), 1.40 ppm (s, 18H, *t*Bu); ^{13}C NMR (100 MHz, $CDCl_3$): δ = 162.56, 145.55, 140.69, 138.87, 135.89, 134.70, 133.50, 132.34, 129.24, 128.75, 126.48, 121.59, 121.45, 119.87, 42.86, 38.98, 32.22, 21.16 ppm; HRMS (ESI): Calculated for $C_{37}H_{40}S_2 + Na^+$ $[M + Na]^+$ 571.2464; found: 571.2462.

1,4-Bis[bis(3-methylthio-1-azulenyl)methyl]benzene (**7a**): the procedure used for the preparation of **6a** was adopted here. Reaction of **5a** (527 mg, 3.03 mmol) and terephthalaldehyde (67 mg, 0.50 mmol) in acetic acid (15 mL) at 50 °C for 24 h, followed by column chromatography on silica gel with CH_2Cl_2 to afford **7a** (347 mg, 87%) as dark green crystals. M.p. 183.5–187.0 °C (CH_2Cl_2); IR (KBr disk): ν_{max} = 3019 (w), 2919 (w), 1572 (s), 1504 (m), 1489 (w), 1449 (w), 1418 (w), 1395 (m), 1377 (m), 1333 (w), 1312 (w), 1217 (w), 1022 (w), 961 (w), 943 (w), 772 (w), 749 (m), 729 (s), 559 (w) cm^{-1}; UV–Vis (CH_2Cl_2): λ_{max} (log ε) = 242 (4.89), 291 (5.04), 299 (5.03), 321 sh (4.61), 363 sh (4.31), 374 (4.34), 614 (3.08), 647 sh (3.07) nm; ^{1}H NMR (400 MHz, $CDCl_3$): δ = 8.55 (d, 4H, *J* = 9.6 Hz, H-8), 8.16 (d, 4H, *J* = 9.6 Hz, H-4), 7.54 (t, 4H, *J* = 9.6 Hz, H-6), 7.45 (s, 4H, H-2), 7.15 (t, 4H, *J* = 9.6 Hz, H-7), 7.05 (s, 4H, Ph), 7.00 (t, 4H, *J* = 9.6 Hz, H-5), 6.62 (s, 2H, CH), 2.36 (s, 12H, SCH_3) ppm; Low solubility hampered the measurement of ^{13}C NMR. HRMS (ESI): Calculated for $C_{52}H_{42}S_4 + Na^+$ $[M + Na]^+$ 817.2062; found: 817.2056.

1,4-Bis[bis(6-*tert*-butyl-3-methylthio-1-azulenyl)methyl]benzene (**7b**): the procedure used for the preparation of **6a** was adopted here. Reaction of **5b** (1.98 g, 8.59 mmol) and terephthalaldehyde (196 mg, 1.46 mmol) in acetic acid (20 mL) and CH_2Cl_2 (2 mL) at room temperature for 24 h, followed by column chromatography on silica gel with CH_2Cl_2 to afford **7b** (1.42 g, 95%) as green crystals. M.p. > 300 °C (CH_2Cl_2); IR (KBr disk): ν_{max} = 2963 (m), 2917 (w), 2869 (w), 1578 (s), 1549 (w), 1505 (w), 1408 (w), 1362 (w), 1337 (w), 1308 (w), 1252 (w), 1067 (w), 1021 (w), 965 (w), 835 (m), 822 (w), 675 (w), 588 (w), 450 (w) cm^{-1}; UV–Vis (CH_2Cl_2): λ_{max} (log ε) = 241 (4.89), 296 sh (5.15), 305 (5.18), 360 (4.36), 376 (4.36), 601 (3.15) nm; ^{1}H NMR (400 MHz, $CDCl_3$): δ = 8.48 (d, 4H, *J* = 10.0 Hz, H-4), 8.13 (d, 4H, *J* = 10.0 Hz, H-8), 7.39 (s, 4H, H-2), 7.33 (dd, 4H, *J* = 10.0, 1.2 Hz, H-5), 7.17 (dd, 4H, *J* = 10.0, 1.2 Hz, H-7), 7.06 (s, 4H, Ph), 6.58 (s, 2H, CH), 2.35 (s, 12H, SCH_3), 1.39 (s, 36H, *t*Bu) ppm; ^{13}C NMR (100 MHz, $CDCl_3$): δ = 145.37, 141.33, 140.10, 138.90, 137.16, 135.93, 134.48, 132.67, 129.27, 128.92, 126.74, 123.45, 123.42, 120.85, 43.14, 20.99, 15.78 ppm; HRMS (ESI): Calculated for $C_{68}H_{74}S_4 + Na^+$ $[M + Na]^+$ 1041.4566; found: 1041.4560.

General Procedure for the Preparation of Hexafluorophosphates **3a,b**$^{+}\cdot PF_6^-$ and **4a,b**$^{2+}\cdot 2PF_6^-$: DDQ was added to a solution of **6a**, **6b**, **7a**, and **7b** in CH_2Cl_2 and the solution was stirred at room temperature for 30 min. 60% HPF_6 solution was added to the mixture and stirred for an additional 15 min. Water was added to the mixture and the resulting suspension was collected by filtration. The filtrate was also extracted with CH_2Cl_2, washed with water, dried with $MgSO_4$, and concentrated under reduced pressure. The residue was crystallized from CH_2Cl_2 and Et_2O. The precipitated crystals were collected by filtration and washed with Et_2O to give the corresponding cations **3a⁺**, **3b⁺**, **4b²⁺**, and **4b²⁺** as hexafluorophosphates.

Bis(3-methylthio-1-azulenyl)phenylmethylium Hexafluorophosphate (**3a**$^+$·PF_6^-): the general procedure was followed using DDQ (65 mg, 0.29 mmol), **6a** (104 mg, 0.24 mmol), and 60% HPF_6 (5 mL) in CH_2Cl_2 (25 mL). Recrystallization from CH_2Cl_2/ether gave **3a**$^+$·PF_6^- (131 mg, 99%) as dark green crystals. M.p. > 300 °C (decomp.); IR (KBr disk): ν_{max} = 2923 (w), 1592 (w), 1570 (w), 1538 (w), 1470 (s), 1437 (m), 1408 (s), 1325 (s), 1310 (s), 1277 (s), 1227 (m), 1200 (w), 1090 (w), 999 (w), 968 (w), 922 (w), 878 (m), 839 (s), 739 (w), 693 (w), 596 (w), 558 (m), 486 (w), 453 (w), 434 (w) cm^{-1}; UV–Vis (CH_3CN): λ_{max} (log ε) = 235 (4.68), 254 sh (4.62), 295 (4.60), 370 (4.37), 422 (4.17), 518 sh (3.78), 740 (4.44) nm; UV–Vis (CH_2Cl_2): λ_{max} (log ε) = 237 (4.60), 256 sh (4.58), 300 (4.54), 376 (4.36), 428 (4.18), 521 sh (3.75), 755 (4.44) nm; UV–Vis (Hexane): λ_{max} (log ε) = 266 sh (4.54), 300 (4.49), 367 (4.35), 427 (4.21), 671 sh (4.30), 733 (4.42) nm; ^{1}H NMR (400 MHz, CD_3CN): δ = 8.80 (dd, 2H, *J* = 10.0, 1.2 Hz, H-4), 8.16 (t, 2H, *J* = 10.0 Hz, H-6), 8.05 (ddd, 2H, *J* = 10.0, 0.8, 0.8 Hz, H-5), 7.93 (dd, 2H, *J* = 10.0, 0.8 Hz, H-8), 7.84 (s, 2H, H-2), 7.83 (tt, 1H, *J* = 8.0, 1.2 Hz, *p*-Ph), 7.64 (ddd, 2H, *J* = 8.0, 1.2, 1.2 Hz, *m*-Ph), 7.57 (ddd, 2H, *J* = 10.0, 0.8, 0.8 Hz, H-7), 7.50 (dd, 2H, *J* = 8.0, 1.2 Hz, *o*-Ph), 2.61 ppm (s, 6H, SCH_3) ppm; ^{13}C NMR (100 MHz, CD_3CN): δ = 160.30, 151.35, 150.45, 145.75, 143.72, 143.13, 141.49, 140.26, 136.56, 136.46, 136.44, 136.38, 134.71, 134.53, 130.52, 17.69 ppm; HRMS (ESI): Calculated for $C_{29}H_{23}S_2^+$ $[M - PF_6]^+$ 435.1241; found: 435.1241.

Bis(6-*tert*-butyl-3-methylthio-1-azulenyl)phenylmethylium Hexafluorophosphate (**3b**$^+$·PF_6^-): the general procedure was followed by using DDQ (272 mg, 1.20 mmol), **6b** (549 mg, 1.00 mmol), and 60% HPF_6 (10 mL) in CH_2Cl_2 (50 mL). Recrystallization from CH_2Cl_2/ether gave **3b**$^+$·PF_6^- (630 mg, 91%) as dark green crystals. M.p. 168.0–175.0 °C (decomp.); IR (KBr disk): ν_{max} = 2963 (w), 2872 (w), 1572 (w), 1497 (w), 1470 (s), 1441 (m), 1416 (s), 1370 (w), 1347 (m), 1323 (s), 1294 (s), 1244 (s), 1192 (m), 1111 (m), 1075 (m), 870 (w), 839 (s), 733 (w), 704 (w), 558 (m) cm^{-1}; UV–Vis (CH_3CN): λ_{max} (log ε) = 258 (4.57), 304 (4.55), 370 (4.31), 426 (4.13), 515 sh (3.74), 740 (4.40) nm; UV–Vis (CH_2Cl_2): λ_{max} (log ε) = 261 (4.55), 306 (4.54), 376 (4.29), 429 (4.11), 515 sh (3.73), 738 (4.40) nm; UV-Vis (Hexane): λ_{max} (log ε) = 262 (4.55), 306 (4.52), 362 (4.29), 424 (4.02), 672 sh (4.30), 723 (4.38) nm; ^{1}H NMR (400 MHz, CD_3CN): δ = 8.69 (d, 2H, *J* = 10.4 Hz, H-4), 8.23 (dd, 2H, *J* = 10.4, 0.8 Hz, H-5), 7.80 (t, 1H, *J* = 7.6 Hz, *p*-Ph), 7.78 (d, 2H, *J* = 10.8 Hz, H-8), 7.71 (dd, 2H, *J* = 10.4, 0.8 Hz, H-7), 7.70 (s, 2H, H-2), 7.63 (t, 2H, *J* = 7.6 Hz, *m*-Ph), 7.50 (d, 2H, *J* = 7.6 Hz, *o*-Ph), 2.58 (s, 6H, SCH_3), 1.40 (s, 18H, 6-*t*Bu) ppm; ^{13}C NMR (100 MHz, CD_3CN): δ = 171.37, 159.23, 150.07, 148.90, 143.10, 142.78, 140.46, 138.96, 136.23, 135.64, 134.95, 134.46, 134.34, 134.18, 130.42, 40.78, 32.08, 17.86 ppm; HRMS (ESI): Calculated for $C_{37}H_{39}S_2^+$ $[M - PF_6]^+$ 547.2488; found: 547.2488.

1,4-Phenylenebis[bis(3-methylthio-1-azulenyl)methylium] Bis(hexafluorophosphate) (**4a**$^{2+}$·$2PF_6^-$): the general procedure was followed by using DDQ (36 mg, 0.16 mmol), **7a** (52 mg, 0.065 mmol), and 60% HPF_6 (4 mL) in CH_2Cl_2 (30 mL). Recrystallization from CH_2Cl_2/ether gave **4a**$^{2+}$·$2PF_6^-$ (65 mg, 91%) as dark green crystals. M.p. > 300 °C (decomp.); IR (KBr disk): ν_{max} = 2960 (w), 1472 (m), 1437 (w), 1408 (m), 1325 (s), 1308 (s), 1277 (s), 1229 (m), 1086 (w), 968 (w), 926 (w), 878 (w), 837 (s), 760 (w), 739 (w), 691 (w), 558 (m), 509 (w), 455 (w) cm^{-1}; UV-Vis (CH_3CN): λ_{max} (log ε) = 236 (4.82), 255 (4.82), 298 (4.76), 376 (4.46), 423 (4.49), 607 (4.29), 773 (4.55) nm; UV–Vis (CH_2Cl_2): λ_{max} (log ε) = 260 (4.83), 302 (4.77), 382 (4.51), 428 (4.50), 612 sh (4.31), 785 (4.55) nm; UV–Vis (Hexane): λ_{max} (log ε) = 259 (4.60), 306 (4.52), 384 (4.39), 442 (4.32), 634 sh (4.19) nm; ^{1}H NMR (400 MHz, CD_3CN): δ = 8.80 (d, 4H, *J* = 9.6 Hz, H-4), 8.22 (t, 4H, *J* = 9.6 Hz, H-6), 8.11 (d, 4H, *J* = 9.6 Hz, H-8), 8.09 (t, 4H, *J* = 9.6 Hz, H-5), 7.99 (s, 4H, H-2), 7.70 (s, 4H, Ph), 7.66 (t, 4H, *J* = 9.6 Hz, H-7), 2.67 (s, 12H, SCH_3) ppm; ^{13}C NMR (100 MHz, CD_3CN): δ = 156.92, 151.52, 150.56, 146.92, 146.03, 143.09, 141.73, 140.37, 137.33, 137.02, 136.92, 136.72, 134.98, 17.58 ppm; HRMS (ESI): Calculated for $C_{52}H_{40}S_4^{2+}$ $[M - 2PF_6]^{2+}$ 396.1001; found: 396.1001.

1,4-Phenylenebis[bis(6-*tert*-butyl-3-methylthio-1-azulenyl)methylium] Bis(hexafluorophosphate) (**4b**$^{2+}$·$2PF_6^-$): the general procedure was followed by using DDQ (60 mg, 0.26 mmol), **7b**

(109 mg, 0.11 mmol), and 60% HPF_6 (5 mL) in CH_2Cl_2 (25 mL). Recrystallization from CH_2Cl_2/ether gave **4b**$^{2+}\cdot 2PF_6^-$ (128 mg, 99%) as dark green crystals. M.p. 252.0–257.0 °C (CH_2Cl_2/ether); IR (KBr disk): ν_{max} = 2965 (w), 2872 (w), 1574 (m), 1497 (m), 1472 (s), 1443 (s), 1416 (s), 1370 (m), 1320 (s), 1296 (s), 1246 (s), 1194 (m), 1111 (m), 1076 (m), 1044 (w), 972 (w), 924 (w), 839 (s), 737 (w), 700 (w), 558 (m), 507 (w), 469 (w) cm^{-1}; UV-Vis (CH_3CN): λ_{max} (log ε) = 236 (4.85), 264 (4.88), 303 (4.89), 386 sh (4.55), 416 (4.57), 604 (4.33), 766 (4.62) nm; UV–Vis (CH_2Cl_2): λ_{max} (log ε) = 266 (4.79), 307 (4.80), 385 (4.50), 424 (4.50), 612 sh (4.31), 777 (4.54) nm; UV–Vis (Hexane): λ_{max} (log ε) = 265 (4.65), 306 (4.67), 424 (4.41), 766 (4.44) nm; ^{1}H NMR (400 MHz, CD_3CN): δ = 8.73 (d, 4H, *J* = 10.8 Hz, H-4), 8.28 (dd, 4H, *J* = 10.8, 2.0 Hz, H-5), 7.92 (s, 4H, H-2), 7.88 (d, 4H, *J* = 10.8 Hz, H-8), 7.76 (dd, 4H, *J* = 10.8, 2.0 Hz, H-7), 7.75 (s, 4H, Ph), 2.66 (s, 12H, SCH_3), 1.42 (s, 36H, *t*-Bu) ppm; ^{13}C NMR (100 MHz, CD_3CN): δ = 171.67, 155.99, 150.23, 148.98, 146.87, 142.16, 140.56, 139.08, 136.48, 136.36, 135.31, 134.95, 134.60, 40.88, 32.09, 17.82; HRMS (ESI): Calculated for $C_{63}H_{72}S_4^{2+}$ $[M - 2PF_6]^{2+}$ 508.2253; found: 508.2253.

4. Conclusions

In summary, we have prepared cations **3a**,**b**$^{+}\cdot PF_6^-$ and dications **4a**,**b**$^{2+}\cdot 2PF_6^-$ and clarified their properties. Although the pK_R^+ values of **3a**,**b**$^{+}\cdot PF_6^-$ and **4a**,**b**$^{2+}\cdot 2PF_6^-$ indicated a lower thermodynamic stability compared with **1**$^{+}\cdot PF_6^-$ and dications **2**$^{2+}\cdot 2PF_6^-$, these cations still exhibited high pK_R^+ values, indicating high thermodynamic stability. These observations indicate the less effective stabilization of the methylthio moiety compared with that of the *tert*-butyl groups at the same position. The CV experiments showed that **3a**,**b**$^{+}\cdot PF_6^-$ and **4a**,**b**$^{2+}\cdot 2PF_6^-$ exhibited a reversible reduction wave. Furthermore, a noticeable color change was observed during the electrochemical reduction of **3a**,**b**$^{+}\cdot PF_6^-$ and **4a**,**b**$^{2+}\cdot 2PF_6^-$. In particular, **4a**,**b**$^{2+}\cdot 2PF_6^-$ displayed a remarkable color change resulting from the formation of the quinoidal structures **8a**,**b**. These facts indicate that **4a**,**b**$^{2+}\cdot 2PF_6^-$ served as the violene–cyanine hybrid in terms of a one-step two-electron reduction to generate a quinoidal form.

Supplementary Materials: The following supporting information can be downloaded at: https://www.mdpi.com/article/10.3390/org3040034/s1, Supplementary File S1: charts of ^{1}H NMR, ^{13}C NMR and COSY spectra, Supplementary File S2: UV–Vis spectra, Supplementary File S3: continuous change in the visible spectra and their photos, and Supplementary File S4: cyclic voltammograms of **3a**,**b**$^{+}\cdot PF_6^-$ and **4a**,**b**$^{2+}\cdot 2PF_6^-$.

Author Contributions: Conceptualization, T.S.; methodology, T.S. and N.S.; formal analysis, T.S., N.S., R.S. and S.I.; investigation, T.S., N.S., R.S. and S.I.; resources, T.S., N.S., R.S. and S.I.; writing–original draft preparation, T.S.; writing–review and editing, T.S., N.S., R.S. and S.I.; supervision, T.S.; funding acquisition, T.S. All authors have read and agreed to the published version of the manuscript.

Funding: This work was supported by JSPS KAKENHI Grant Number 21K05037.

Conflicts of Interest: The authors declare no conflict of interest.

References

1. Zeller, K.-P. Azulene in Methoden. *Org. Chem.* **1952**, *V Pt 2c*, 127–418.
2. Ito, S.; Morita, N. Creation of Stabilized Electrochromic Materials by Taking Advantage of Azulene Skeletons. *Eur. J. Org. Chem.* **2009**, *2009*, 4567–4579. [CrossRef]
3. Ito, S.; Shoji, T.; Morita, N. Recent Advances in the Development of Methods for the Preparation of Functionalized Azulenes for Electrochromic Applications. *Synlett* **2011**, *16*, 2279–2298. [CrossRef]
4. Shoji, T.; Ito, S. The Preparation and Properties of Heteroarylazulenes and Hetero-Fused Azulenes. *Adv. Heterocycl. Chem.* **2018**, *126*, 1–54.
5. Shoji, T.; Okujima, T.; Ito, S. Development of Heterocycle-Substituted and Fused Azulenes in the Last Decade (2010–2020). *Int. J. Mol. Sci.* **2020**, *21*, 7087. [CrossRef] [PubMed]
6. Shoji, T.; Ito, S.; Yasunami, M. Synthesis of Azulene Derivatives from 2*H*-Cyclohepta[*b*]furan-2-ones as StartingMaterials: Their Reactivity and Properties. *Int. J. Mol. Sci.* **2021**, *22*, 10686. [CrossRef]
7. Tomiyama, T.; Wakabayashi, S.; Kosakai, K.; Yokota, M. Azulene derivatives: New non-prostanoid thromboxane A2 receptor antagonists. *J. Med. Chem.* **1990**, *33*, 2323–2326. [CrossRef]

8. Tomiyama, T.; Yokota, M.; Wakabayashi, S.; Kosakai, K.; Yanagisawa, T. Design, synthesis, and pharmacology of 3-substituted sodium azulene-1-sulfontes and related compounds: Non-prostanoid thromboxane A2 receptor antagonists. *J. Med. Chem.* **1993**, *36*, 791–800. [CrossRef]
9. Nakamura, H.; Sekido, M.; Yamamoto, Y. Synthesis of Carboranes Containing an Azulene Framework and in vitro Evaluation as Boron Carriers. *J. Med. Chem.* **1997**, *40*, 2825–2830. [CrossRef]
10. Rekka, E.; Chrysselis, M.; Siskou, I.; Kourounakis, A. Synthesis of New Azulene Derivatives and Study of Their Effect on Lipid Peroxidation and Lipoxygenase Activity. *Chem. Pharm. Bull.* **2002**, *50*, 904–907. [CrossRef]
11. Ito, S.; Kikuchi, S.; Okujima, T.; Morita, N.; Asao, T. Synthesis, Properties, and Redox Behavior of Di(1-azulenyl)(2- and 3-thienyl)methyl Cations and Dications Composed of Two Di(1-azulenyl)methylium Units Connected with 2,5-Thiophenediyl and 2,5-Thienothiophenediyl Spacers. *J. Org. Chem.* **2001**, *66*, 2470–2479. [CrossRef] [PubMed]
12. Ito, S.; Nomura, A.; Morita, N.; Kabuto, C.; Kobayashi, H.; Maejima, S.; Fujimori, K.; Yasunami, M. Synthesis and Two-Electron Redox Behavior of Diazuleno[2,1-*a*:1,2-*c*]naphthalenes. *J. Org. Chem.* **2002**, *67*, 7295–7302. [CrossRef] [PubMed]
13. Ito, S.; Inabe, H.; Morita, N.; Ohta, K.; Kitamura, T.; Imafuku, K. Synthesis of Poly(6-azulenylethynyl)benzene Derivatives as a Multielectron Redox System with Liquid Crystalline Behavior. *J. Am. Chem. Soc.* **2003**, *125*, 1669–1680. [CrossRef] [PubMed]
14. Ito, S.; Kubo, T.; Morita, N.; Ikoma, T.; Tero-Kubota, S.; Kawakami, J.; Tajiri, A. Azulene-Substituted Aromatic Amines. Synthesis and Amphoteric Redox Behavior of *N*,*N*-Di(6-azulenyl)-*p*-toluidine and *N*,*N*,*N*′,*N*′-Tetra(6-azulenyl)-*p*-phenylenediamine and Their Derivatives. *J. Org. Chem.* **2005**, *70*, 2285–2293. [CrossRef] [PubMed]
15. Ito, S.; Akimoto, K.; Kawakami, J.; Tajiri, A.; Shoji, T.; Satake, H.; Morita, N. Synthesis, Stabilities, and Redox Behavior of Mono-, Di-, and Tetracations Composed of Di(1-azulenyl)methylium Units Connected to a Benzene Ring by Phenyl- and 2-Thienylacetylene Spacers. A Concept of a Cyanine−Cyanine Hybrid as a Stabilized Electrochromic System. *J. Org. Chem.* **2007**, *72*, 162–172.
16. Shoji, T.; Ito, S.; Toyota, K.; Yasunami, M.; Morita, N. Synthesis, Properties, and Redox Behavior of Mono-, Bis-, and Tris[1,1,4,4,-tetracyano-2-(1-azulenyl)-3-butadienyl] Chromophores Binding with Benzene and Thiophene Cores. *Chem. Eur. J.* **2008**, *14*, 8398–8408. [CrossRef]
17. Shoji, T.; Ito, S.; Toyota, K.; Iwamoto, T.; Yasunami, M.; Morita, N. Reactions between 1-Ethynylazulenes and 7,7,8,8-Tetracyanoquinodimethane (TCNQ): Preparation, Properties, and Redox Behavior of Novel Azulene-Substituted Redox-Active Chromophores. *Eur. J. Org. Chem.* **2009**, *2009*, 4316–4324. [CrossRef]
18. Shoji, T.; Ito, S.; Okujima, T.; Morita, N. Synthesis of 2-Azulenyl-1,1,4,4-tetracyano-3-ferrocenyl-1,3-butadienes by [2+2] Cycloaddition of (Ferrocenylethynyl)azulenes with Tetracyanoethylene. *Chem. Eur. J.* **2013**, *19*, 5721–5730. [CrossRef]
19. Shoji, T.; Maruyama, M.; Shimomura, E.; Maruyama, A.; Ito, S.; Okujima, T.; Toyota, K.; Morita, N. Synthesis, Properties, and Redox Behavior of Tetracyanobutadiene and Dicyanoquinodimethane Chromophores Bearing Two Azulenyl Substituents. *J. Org. Chem.* **2013**, *78*, 12513–12524. [CrossRef]
20. Shoji, T.; Maruyama, M.; Maruyama, A.; Ito, S.; Okujima, T.; Toyota, K. Synthesis of 1,3-bis(tetracyano-2-azulenyl-3-butadienyl)azulenes by the [2+2] cycloaddition-retroelectrocyclization of 1,3-bis(azulenylethynyl)azulenes with tetracyanoethylene. *Chem. Eur. J.* **2014**, *20*, 11903–11912. [CrossRef]
21. Shoji, T.; Ito, S. Azulene-Based Donor–Acceptor Systems: Synthesis, Optical, and Electrochemical Properties. *Chem. Eur. J.* **2017**, *23*, 16696–16709. [CrossRef] [PubMed]
22. Ito, S.; Morita, N.; Asao, T. Synthesis, Properties, and Redox Behaviors of Di- and Trications Composed of Di(1-azulenyl)methylium Units Connected by *p*- and *m*-Phenylene and 1,3,5-Benzenetriyl Spacers. *Bull. Chem. Soc. Jpn.* **2000**, *73*, 1865–1874. [CrossRef]
23. Shoji, T.; Higashi, J.; Ito, S.; Toyota, K.; Yasunami, M.; Fujimori, K.; Asao, T.; Morita, N. Synthesis and Redox Behavior of 1-Azulenyl Sulfides and Efficient Synthesis of 1,1′-Biazulenes. *Eur. J. Org. Chem.* **2008**, *2008*, 1242–1252. [CrossRef]
24. Shoji, T.; Maruyama, A.; Maruyama, M.; Ito, S.; Okujima, T.; Higashi, J.; Toyota, K.; Morita, N. Synthesis and Properties of 6-Methoxy- and 6-Dimethylamino-1-methylthio- and 1,3-Bis(methylthio)azulenes and Triflic Anhydride-Mediated Synthesis of Their Biaryl Derivatives. Synthesis and Properties of 6-Methoxy- and 6-Dimethylamino-1-methylthio- and 1,3-Bis(methylthio)azulenes and Triflic Anhydride-Mediated Synthesis of Their Biaryl Derivatives. *Bull. Chem. Soc. Jpn.* **2014**, *87*, 141–154.
25. Shoji, T.; Ito, S.; Toyota, K.; Yasunami, M.; Morita, N. The novel transition metal free synthesis of 1,1′-biazulene. *Tetrahedron Lett.* **2007**, *48*, 4999–5002. [CrossRef]
26. Higashi, J.; Shoji, T.; Ito, S.; Toyota, K.; Yasunami, M.; Morita, N. Heteroarylation of 1-Azulenyl Methyl Sulfide: Two-Step Synthetic Strategy for 1-Methylthio-3-(heteroaryl)azulenes Using the Triflate of N-Containing Heterocycles. *Eur. J. Org. Chem.* **2008**, *2008*, 5823–5831. [CrossRef]
27. Shoji, T.; Ito, S.; Toyota, K.; Iwamoto, T.; Yasunami, M.; Morita, N. Synthesis and Redox Behavior of 1,3-Bis(methylthio-) and 1,3-Bis(phenylthio)azulenes Bearing 2- and 3-Thienyl Substituents by Palladium-Catalyzed Cross-Coupling Reaction of 2- and 6-Haloazulenes with Thienylmagnesium Ate Complexes. *Eur. J. Org. Chem.* **2009**, *2009*, 4307–4315. [CrossRef]
28. Shoji, T.; Higashi, H.; Ito, S.; Morita, N. Synthesis, Properties, and Redox Behavior of Ferrocene-Substituted Bis(3-methylthio-1-azulenyl)methylium Ions. *Eur. J. Inorg. Chem.* **2010**, *2010*, 4886–4891. [CrossRef]
29. Kirby, E.C.; Reid, D.H. Conjugated cyclic hydrocarbons and their heterocyclic analogues. Part II. The condensation of azulenes with homocyclic and heterocyclic aromatic aldehydes in the presence of perchloric acid. *J. Chem. Soc.* **1960**, 494–501. [CrossRef]

30. Kirby, E.C.; Reid, D.H. Conjugated cyclic hydrocarbons and their heterocyclic analogues. Part V. 1-1′-Azulenylmethyleneazulenium salts and 1-ethoxymethyl-eneazulenium salts. *J. Chem. Soc.* **1961**, 1724–1730. [CrossRef]
31. Kirby, E.C.; Reid, D.H. Conjugated cyclic hydrocarbons and their heterocyclic analogues. Part VI. The condensation of azulenes with aliphatic aldehydes in the presence of perchloric acid. *J. Chem. Soc.* **1961**, 3579–3593. [CrossRef]
32. Takekuma, S.-i.; Takekuma, H.; Matsubara, Y.; Hirai, A.; Yamamoto, H.; Nozoe, T. Reactions of Guaiazulene with Aldehyde Reagents in Acetic Acid—An Efficient Preparation of 3,3′-Methylenediguaiazulene Derivatives. *Nippon Kagaku Kaishi* **1996**, *1996*, 419–423. [CrossRef]
33. Takekuma, S.-i.; Takekuma, H.; Hanaoka, Y.; Yamamoto, H. Reactions of Azulene with Heteroaromatic Carbaldehydes in Acetic Acid. *Nippon Kagaku Kaishi* **1996**, *1996*, 659–662. [CrossRef]
34. Takekuma, S.-i.; Takekuma, H.; Hatanaka, Y.; Kawaguchi, J.; Yamamoto, H. Reactions of Guaiazulene with Phthalaldehyde, Isophthalaldehyde and Terephthalaldehyde in Acetic Acid. *Nippon Kagaku Kaishi* **1998**, *1998*, 275–279. [CrossRef]
35. Takekuma, S.-i.; Sasaki, M.; Takekuma, H.; Yamamoto, H. Preparation and Characteristic Properties of 1,4-Bis(3-guaiazulenylmethylium)benzene Bishexafluorophosphate. *Chem. Lett.* **1999**, *28*, 999–1000. [CrossRef]
36. Ito, S.; Morita, N.; Asao, T. Azulene analogues of triphenylmethyl cation; extremely stable hydrocarbon carbocations. *Tetrahedron Lett.* **1991**, *32*, 773–776. [CrossRef]
37. Cowper, P.; Pockett, A.; Kociok-Köhn, G.; Cameron, P.J.; Lewis, S.E. Azulene-Thiophene-Cyanoacrylic acid dyes with donor-π-acceptor structures. Synthesis, characterisation and evaluation in dye-sensitized solar cells. *Tetrahedron* **2018**, *74*, 2775–2786. [CrossRef]
38. Suppan, P.; Ghoneim, N. *Solvatochromism, The Royal Society of Chemistry*; Londres: Cambridge, UK, 1997.
39. Suppan, P. Invited review solvatochromic shifts: The influence of the medium on the energy of electronic states. *J. Photochem. Photobiol. A* **1990**, *50*, 293–330. [CrossRef]
40. Christian, R. *Solvent and Solvent Effects in Organic Chemistry*; Wiley-VCH: New York, NY, USA, 2004.
41. Takekuma, S.-I.; Sasaki, M.; Takekuma, H.; Yamamoto, H. The isolation of quinoid compound was accomplished by Takekuma. An Efficient Preparation and Characteristic Properties of Tetramethyl 3,3′,3″,3‴-(p–Quinodimethane-7,7,8,8-tetrayltetraazulene-1,1′,1″,1‴-tetracarboxylate. *Nippon Kagaku Kaishi* **2000**, *2000*, 107–114. [CrossRef]
42. Komatsu, K.; Ohta, K.; Fujimoto, T.; Yamamoto, I. Chromic materials. Part 1.-Liquid-crystalline behaviour and electrochromism in bis(octakis-*n*-alkylphthalocyaninato)lutetium(III) complexes. *J. Mater. Chem.* **1994**, *4*, 533–536. [CrossRef]
43. Rosseinsky, D.R.; Monk, P.M.S. Studies of tetra-(bipyridilium) salts as possible polyelectrochromic materials. *J. Appl. Electrochem.* **1994**, *24*, 1213–1221. [CrossRef]
44. Monk, P.M.S.; Mortimer, R.J.; Rosseinsky, D.R. *Electrochromism and Electrochromic Devices*; Cambridge University Press: Cambridge, UK, 2007.
45. Hünig, S.; Kemmer, M.; Wenner, H.; Perepichka, I.F.; Bäuerle, P.; Emge, A.; Gescheidt, G. Violene/Cyanine Hybrids: A General Structure for Electrochromic Systems. *Chem. Eur. J.* **1999**, *5*, 1969–1973. [CrossRef]
46. Hünig, S.; Kemmer, M.; Wenner, H.; Barbosa, F.; Gescheidt, G.; Perepichka, I.F.; Bäuerle, P.; Emge, A.; Peters, K. Violene/Cyanine Hybrids as Electrochromics Part 2: Tetrakis(4-dimethylaminophenyl)ethene and Its Derivatives. *Chem. Eur. J.* **2000**, *6*, 2618–2632. [CrossRef] [PubMed]
47. Hunig, S.; Perepichka, I.F.; Kemmer, M.; Wenner, H.; Bauerle, P.; Emge, A. Violene/cyanine hybrids as electrochromic systems. Part 3: Heterocyclic onium end groups. *Tetrahedron* **2000**, *56*, 4203–4211. [CrossRef]
48. Hünig, S.; Briehn, C.A.; Bäuerle, P.; Emge, A. Electrochromics by Intramolecular Redox Switching of Single Bonds. *Chem. Eur. J.* **2001**, *7*, 2745–2757. [CrossRef]
49. Hünig, S.; Langels, A.; Schmittel, M.; Wenner, H.; Perepichka, I.F.; Peters, K. Violene/Cyanine Hybrids as Electrochromic Systems: A New Variation of the General Structure. *Eur. J. Org. Chem.* **2001**, *2001*, 1393–1399. [CrossRef]